Supplemental figures and legends

A

```
         10         20         30         40         50         60         70
MVKIMPNLPGLYFLQAYPSEEIWRLFVDGRFWSKENGWRGYESREPGCLNAALESLCSIALQVEKSGEEFELSVD
   80         90        100        110        120        130        140        150
LIKRIHKKCGKKVEELQEKNPGELRTDEPVSFGIPAGRASIKGIEEFLSLVFLTEGGAEFGPGKAGPFGPRFDKN
        160        170        180        190        200        210        220
YFKNLNPEQIPDLAKQIYFDMCKYGHSNTNHFYLAVMKNVDVYLEKITQSYNKEIKTAETLDEKLKIIVKHIRMY
  230        240        250        260        270        280        290        300
EVLHPFRDANGRTFVNNLLNILLMQQGLPPATFYEPNVFDLYSAEELVVVVKEAIFNTVEIIEQSKRKTPITLYG
        310        320        330        340        350        360        370
YHSSLEEQTKFRDMLDSPSYEKIKHMDFSDLNPEKLHLKTQKCLSSLNEQYPLHRGAIYLSDPGEIKLLLSNRNE
  380        390        400        410        420        430        440        450
SQINQQIEQGAPPIYVGKTPAHLAVISGNMAMLDELIAKKADLSLQDYDGKTALHYAAECGNMQIMGKILKVVLS
        460        470        480        490        500        510        520
QEDAIKVLNIKDNHGKTAFHYAAEFGTPELISALTTTEVIQINEPDNSGSSAITLAYKNHKLKIFDELLNSGADI
  530        540        550        560        570        580        590        600
SDELLDAIWARKDKETLGKIIAKNEKILLNKEAFRIAISLGSVSLVKKFLRAGVDIDIPLTKDKATPLMLSINSG
        610        620        630        640        650        660        670
NPKLVSYLLKKGANTRLTDTSGNSVLHYVFYSKAENREALANIITEKDKKLINQPNANGNPPLYNAVVVNDLKMA
  680        690        700        710        720        730        740        750
TILLEMGARVDFEDRLGNNILHSAMRRCDLPIILDIVKKDSTLLHKRNSERRNPFHQALHEMHTFPSSKETEEIH
        760        770        780        790        800        810        820
FMNLSDLLLKEGVDLNKKDIKGKTILDIALSKQYFHLCVKLMKAGAHTNISSPSKFLKNSDANSILERPFKFKND
  830        840        850        860        870        880        890        900
LKKELDNNPLIAMAQINDLYVQIKNNRIRTPTGYAPKEGVSFFKGKSNDAKAHDEVLSVLKELYDSKLTEMLGNL
        910        920        930        940        950
PGEGLEEIKRSQKFFDGELKLLIKNQDISRKVDKKSIQEAVGTSLKLKW
```

B C D

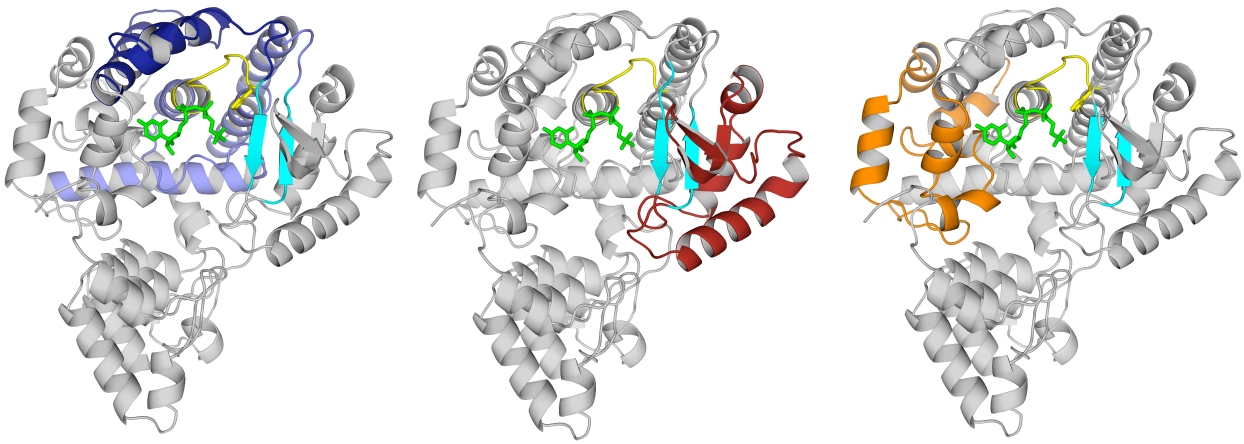

Figure S1. **Domains of AnkX$_{1\text{-}484}$ and prediction of C-terminal ankyrin repeats.**

(A) The sequence of AnkX is color-coded according to the domains described in the text: CMP-binding domain (orange), bipartite FIC domain (in blue, with FIC motif in yellow and β-hairpin in cyan), insert domain (red) and ankyrin repeats (magenta). Ankyrin repeats (α-helices underlined) are observed in the structure up to residue 477. Subsequent ankyrin repeats were predicted by the combined search for ankyrin repeat sequences (REP server, EMBL), automated protein modeling (SWISSMODEL server) and sequence alignment with proteins of

Supplemental figures and legends

known structures (BLAST server). The predicted anti-parallel α-helices are underlined. **(B,C,D)** From left to right: the bipartite FIC domain (N-terminal sub-domain in dark blue, C-terminal sub-domain in light blue) with; the insert domain (red, with β-hairpin in cyan); the CMP-binding domain (orange). The FIC motif is in yellow, the β-hairpin is in cyan and CDP-choline in in green in all panels.

Supplemental figures and legends

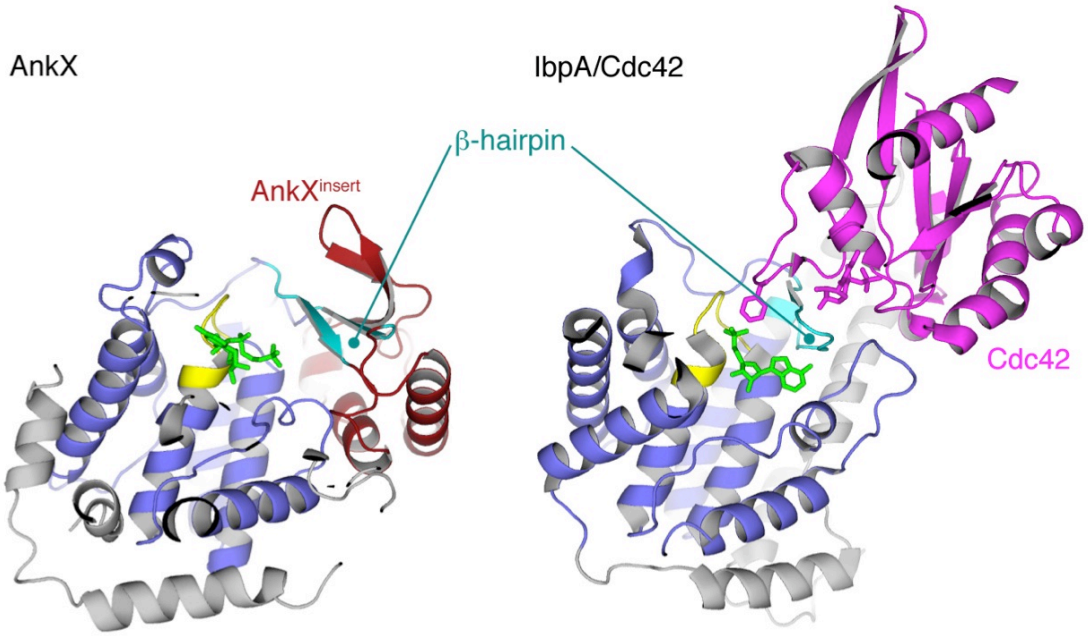

Figure S2. **The β-hairpin of AnkX is unavailable for binding Rab1.**

Comparison of AnkX (left, insert domain in red, CDP-choline in green) and IbpA with bound AMPylated Cdc42 (right, Cdc42 in magenta, AMP in green, taken from PDB 3N3V). The FIC domains (in blue) are shown in the same orientation, with the β-hairpin in cyan.

Supplemental figures and legends

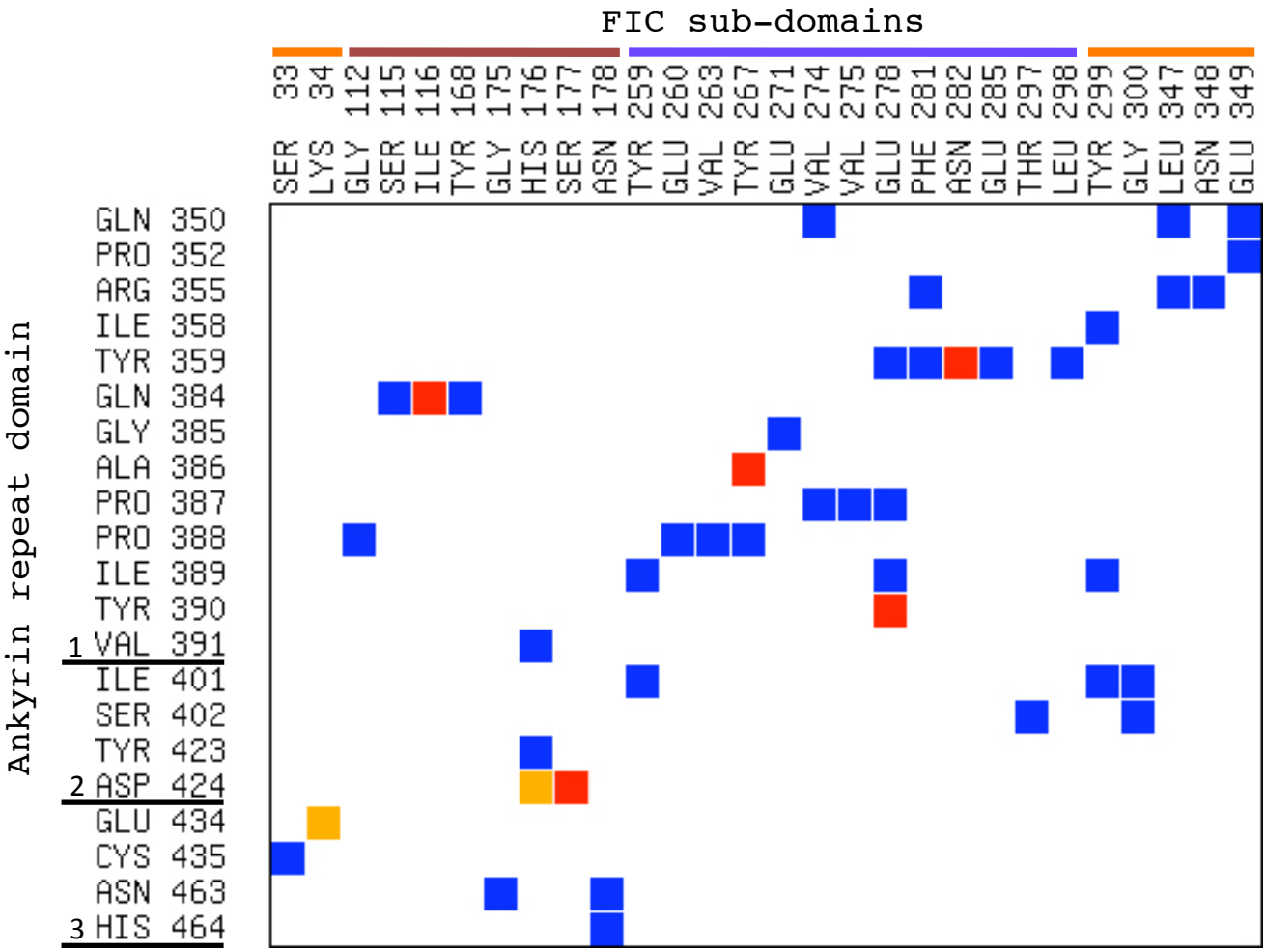

Figure S3. **Intramolecular contacts mediated by the ankyrin repeats.**

Contacts between the residues of the ankyrin repeats (numbered from 1 to 3) and the FIC sub-domains (domain colour-coding as in Fig. S1) are displayed by squares (hydrogen bonds are in red, and salt bridges in orange). Contact map performed using the Contact Map Analysis (CMA) server with a threshold of 10 $Å^2$ (Sobolev V, Eyal E, Gerzon S, Potapov V, Babor M, Prilusky J, Edelman M. (2005) SPACE: a suite of tools for protein structure prediction and analysis based on complementarity and environment. *Nucl. Acids Res.* **33**: W39-W43).

Supplemental figures and legends

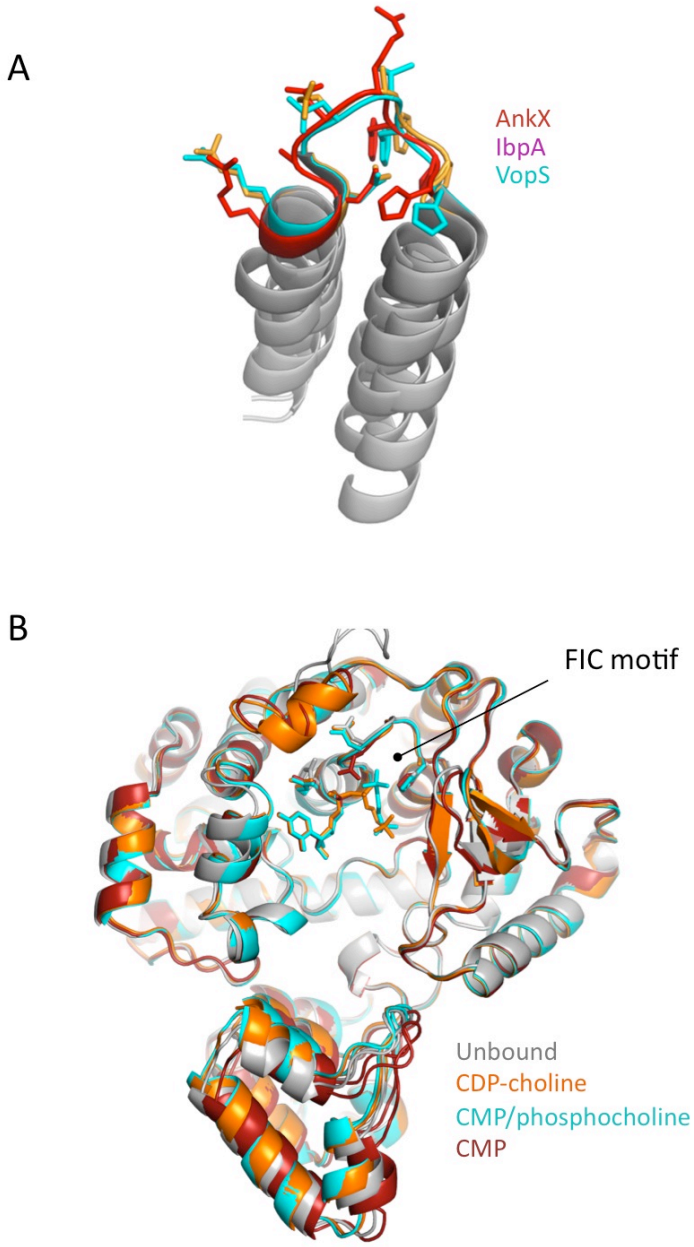

Figure S4. **Conformation of the catalytic FIC motif of AnkX.**

(A) The FIC motif of AnkX has the same conformation as the FIC motifs of AMPylating toxins. **(B)** The conformation of AnkX and the conformation of its active site are the same in unbound, substrate-bound and product bound AnkX structures.

Supplemental figures and legends

A

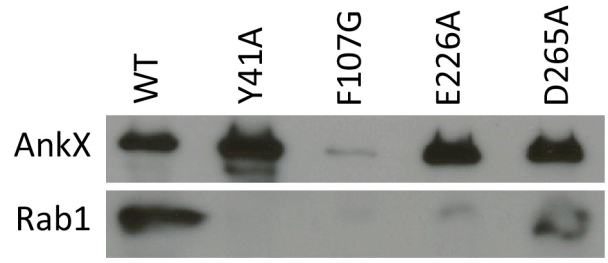

B

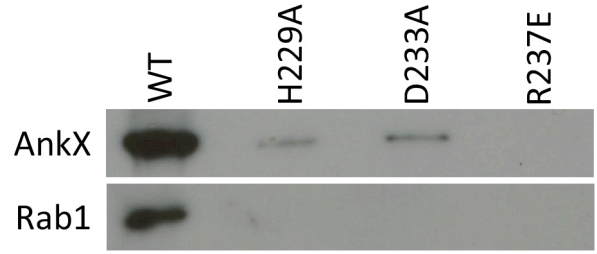

C

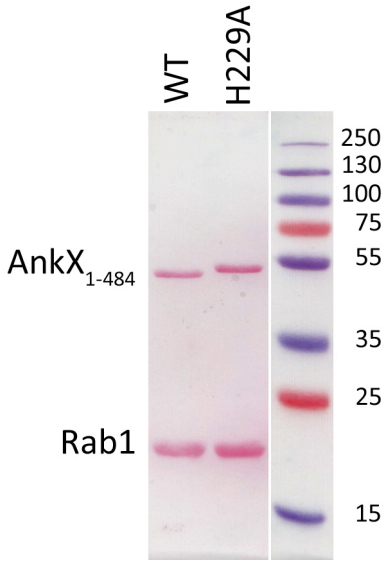

Figure S5. **AnkX auto-phosphocholination and Rab1A phosphocholination by wild-type and mutant AnkX constructs.**

A. Immunoblots of full-length His-tagged AnkX mutants carrying mutations in the CDP-choline binding site. We surmise that differences in binding modalities between the physiological substrate, Rab1, and flexible regions that are the targets of non-specific auto-phosphocholination (see Results and Discussion) explain the difference between Rab1 phosphocholination and auto-phosphocholination than can be seen for some of the AnkX mutants.

B. Immunoblots of full-length His-tagged AnkX mutants carrying mutations in the FIC motif.

C. Ponceau staining of immunoblots of $AnkX_{1-484}$ from Figure 3D.

Supplemental figures and legends

Immunoblots are from *in vitro* reactions that contained full-length His-tagged AnkX mutants and Rab1A in the presence of phosphocholination buffer. Blots were probed with anti-PC antibody to detect phosphocholinated AnkX and Rab1A. Auto-phosphocholination and Rab1-phosphocholination by wild-type AnkX is shown as a control. Densitometry was carried out using the GE Healthcare ImageQuant LAS 4000 gel doc system, which captures chemiluminescence data in the linear stage of the reaction thus providing accurate measurements, and was not done by simply scanning film blots. This makes the quantitation independent of the shape of the quantified band. All mutants are strongly impaired in Rab1 phosphocholination. Most mutants outside the FIC motif retain auto-phosphocholination activity, indicating that they are likely to be properly folded.

Supplemental figures and legends

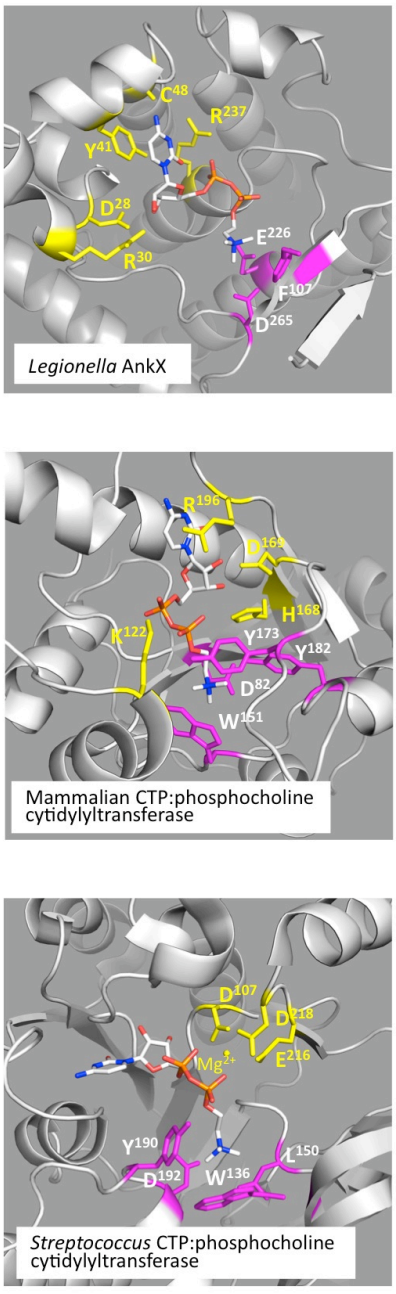

Figure S6. Comparison of the CDP-choline binding sites of *Legionella* AnkX and of bacterial and human CTP-phosphocholine cytidylyltransferases.

CDP-choline is the product of the reaction catalyzed by CTP-phosphocholine cytidylyltransferases, and has been observed in in crystal structures in complex with these enzymes. *Legionella* AnkX (top, this work), mammalian CTP-phosphocholine cytidylyltransferase (middle, PDB entry 3HL4) and *Streptococcus* CTP-phosphocholine cytidylyltransferase (bottom, PDB 1JYL) share a common use of aromatic and negatively charged residues to recognize the choline moiety of CDP-choline, but their

recognition of the CMP moiety is otherwise completely unrelated. The choline moiety is approximately in the same orientation in all views. Residues in contact with the cytidine moiety are in yellow, residues in contact with the choline moiety in magenta. In CTP-phosphocholine cytidylyltransferase structures, the cytosine makes additional interactions with main chain NHs (not shown).

Supplemental figures and legends

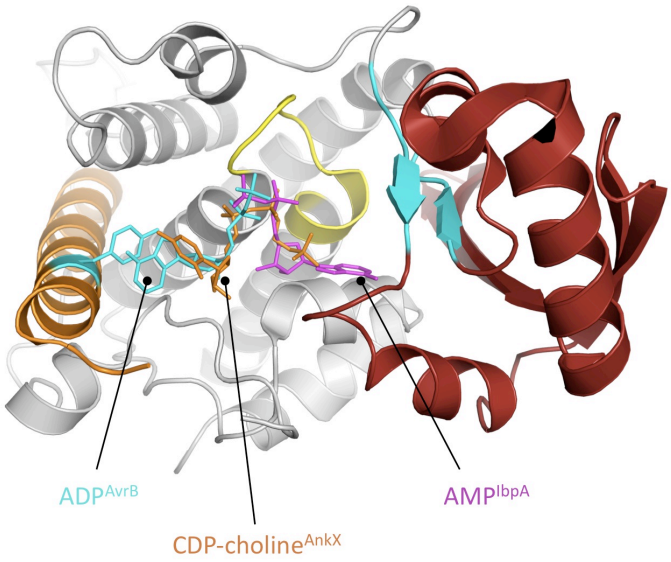

Figure S7. **AvrB binds ADP with the same orientation as the CDP moiety of CDP-choline.** Overall view of the FIC-related AvrB protein with bound ADP in cyan, the atypical FIC motif in yellow and the insert domain in red (from PDB 2NUN). CDP-choline bound to AnkX (in orange) and AMP bound to IbpA (magenta, PDB 3N3V) are overlaid.